AIAA JOURNAL
Vol. 33, No. 8, August 1995

Vortex Shedding and Shear-Layer Instability of Wing at Low-Reynolds Numbers

Rong F. Huang* and Chih L. Lin†
National Taiwan Institute of Technology, Taipei, Taiwan, Republic of China

Flow patterns and characteristics of vortex shedding and shear-layer instability of a NACA 0012 cantilever wing are experimentally studied. Smoke-wire and surface oil-flow techniques are employed to visualize the flow patterns and evolution of vortex shedding. Hot-wire anemometers are used to characterize the frequency domain of the unsteady flow structures. Several characteristic flow modes are classified in the domain of chord Reynolds number and root angle of attack. Effects of the juncture and wing tip are discussed. Vortex shedding can be classified into four characteristic modes. Vortex shedding at low and high angles of attack are found to have different dominant mechanisms. Effects of the juncture and wing tip on the vortex shedding are discussed. Shear-layer instabilities are found to be closely related to the behaviors of the vortex shedding. Behaviors of the shear-layer instabilities can be traced back to the characteristics of the boundary layer on the suction surface of the airfoil.

Nomenclature

C	= chord length of airfoil, 6 cm
d	= Y length of the normal projection of the airfoil on the Y–Z plane
f_s	= frequency of vortex shedding in wake region, Hz
f_t	= frequency of shear-layer instability, Hz
Re_c	= Reynolds number based on chord length of airfoil, $u_w C/\nu$
St	= Strouhal number of vortex shedding, $f_s d/u_w$
u	= local velocity detected by hot-wire anemometer
u_w	= freestream velocity
X	= streamwise coordinate, originated from leading edge of airfoil on root plane
Y	= spanwise coordinate, originated from leading edge of airfoil on root plane
Z	= cross stream coordinate, originated from leading edge of airfoil on root plane
α_0	= root angle of attack
ν	= kinematic viscosity of the air stream

Introduction

THE characteristics of airfoils operating in low-Reynolds number, incompressible flows have been of increasing interest. Many significant aerodynamic problems appear to occur below Reynolds number of about 500,000. The characteristics of the flow over a two-dimensional airfoil at low-Reynolds numbers have been studied by many investigators. Most of the studies were focused on the behavior of the boundary layer on the suction surface, e.g., laminar separation, transition, turbulent reattachment, bubble bursting, etc., due to its significant influence on the aerodynamic performance.[1–11] Lissaman[12] conducted an excellent review of the low-Reynolds number airfoils. Some of the airfoils, e.g., Lissaman 7769, Miley M06-13-128, Wortmann FX63-137, and NACA 63_3-018, exhibit hysteresis loop in aerodynamic performance near the stall, which is closely related to the hysteresis of boundary-layer behavior within a certain range of Reynolds numbers when the airfoils are operated at up- and downstrokes. Other flowfield characteristics having profound influence on the airfoil performance are the vortex shedding in the wake region and the instability wave developed in the shear layer due to the separation of the boundary layer. The origin of the oscillating unsteady flow can be traced back to the boundary-layer behavior on the airfoil surfaces.[13] The von Kármán type vortex street behind an airfoil was discussed by Stuber and Gharib.[14] Of the interesting behaviors related to the shed vortices are the vortex-induced vibration[15] of the airfoil and the lock-on phenomenon[16] of the shedding frequency.

Although the flow characteristics of the two-dimensional low-Reynolds number airfoils have been comprehensively studied by the investigators, a systematic survey of the characteristic flow modes and the unsteady flow structures of the cantilever wing in the Reynolds number/angle of attack domain is still an open area for researchers. In this paper, we present results of an experimental study on the characteristics of the vortex shedding and shear-layer instability of a cantilever finite wing that is subjected to the effects of wing tip and wall boundary layer. The results show not only the characteristics of the flow over the airfoil but also the interaction between the shed vortices and the shear-layer instabilities.

Experimental Setup

The experiments were performed in an open-loop wind tunnel as shown in Fig. 1. The wind tunnel has a test section of 60 × 60 × 120 cm, made of one polished aluminum alloy plate as the floor and three high-transparency acrylic panels as the ceiling and side walls for photography and visualization. The contraction ratio of the nozzle is 10 to 1. The velocity in the test section varies between 0.5 and 52 m/s. The maximum turbulence intensity is less than 0.2% within the operating range. The nonuniformity of the average velocity profile across the cross section is lower than 0.5%. During the experiments the velocity of the approaching flow was monitored with a pitot-static tube. An aluminum plate with sharp leading and trailing edges is placed 5 cm above the floor for control of the boundary-layer thickness.

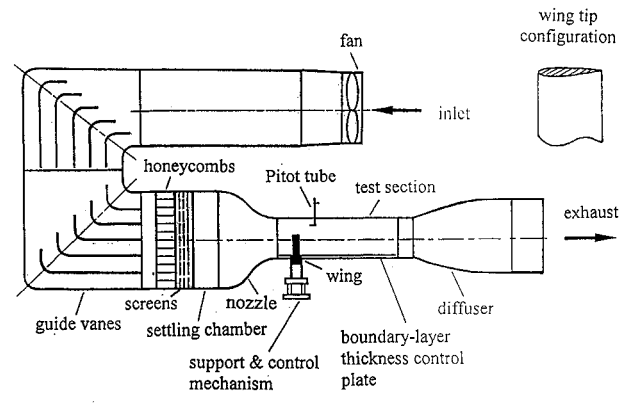

Fig. 1 Experimental setup.

Received July 23, 1994; revision received Feb. 1, 1995; accepted for publication Feb. 23, 1995.

*Associate Professor, Department of Mechanical Engineering. Member AIAA.
†Graduate Student, Department of Mechanical Engineering.

The rectangular airfoil model is made of aluminum. The profile of the cross section is NACA 0012. Chord length is 6 cm and span is 30 cm, which gives an aspect ratio of 5. The wing tip is sharp edged, as shown in Fig. 1. The airfoil model is mounted on a support and protrudes through perpendicularly to the aluminum floor of the test section and the boundary-layer thickness control plate.

The smoke-wire technique together with high-speed photography and video recording are used to visualize the flow separation as well as the vortex evolution for wind velocity lower than 5 m/s ($Re_c = 20{,}000$). For wind velocity higher than 10 m/s ($Re_c = 40{,}000$), the oil-flow technique is employed to record the flow pattern on the suction surface. Two corrugated wolfram wires 80 μm in diameter are used as the smoke wires. One is placed 10 mm upstream the leading edge of the airfoil and the other 0.5 mm downstream the trailing edge. Thin mineral oil is brush coated on the wire surface. The wire is ohmmically heated to generate fine smoke streaks to make the flowfield observable. The surface temperature of the smoke wire is kept as low as possible but still high enough to evaporate the oil so that the buoyancy-induced convection[17] is estimated to be lower than 2.5 cm/s. The condensed vapor aerosols (the smoke) of the thin mineral oil have diameters on the order of 1 μm (Ref. 18). The slip factor and Stokes number[19] for these aerosols are estimated to be about 1.108 and 0.002, respectively. Hence, the smoke streaks are considered to follow the flow properly.

The frequencies of the shed vortices in the wake region and the instability waves developed on the separated shear layers are detected by two one-component hot-wire anemometers. The wire diameter is smaller than 5 μm, which ensures a dynamic response no less than 4000 Hz. The hot-wire signals are fed simultaneously to a fast Fourier transform (FFT) analyzer and a high-speed personal computer-based data acquisition system. The data acquisition system has a sample-and-hold function installed for multichannel acquisition with no phase lag.

The accuracy of the freestream velocity measurement is primarily affected by the alignment of the pitot tube and the calibration of the pressure transducer. With the help of an on-line micropressure calibration system and careful alignment of the pitot tube, the uncertainty of the freestream velocity was estimated to be as large as 3%. The support for the wing model has a resolution of 0.015 deg when revolving. The accuracy of the root angle of attack was controlled within 0.5%. The accuracy of the shedding frequencies depends not only on the response of the the hot-wire anemometer but also on the record length and sampling rate of the FFT analyzer. The uncertainty of the frequency detected is estimated to be within 1.5% in this experiment.

Results and Discussion

Flow Pattern

The domain of the chord Reynolds number/root angle of attack can be classified into several regions that characterize different flow modes. Figure 2 shows the classification of the characteristic flow modes at the plane of $Y/C = 3$, which is basically two dimensional according to the observed flow patterns. The characteristic flow modes for chord Reynolds number lower than 22,000 are obtained from smoke-wire flow visualization, whereas those for chord Reynolds number higher than 38,000 are obtained from the oil-flow pattern on the airfoil surface. The region between the two dashed lines in Fig. 2 represents where both the smoke-wire and oil-flow pattern techniques are invalid; in this region the wind speed is too low to properly drive the oil flow and is too high to obtain unsmeared smoke streaks. The flow modes in the characteristic regions of Fig. 2 are illustrated as follows.

Smoke-Streak Pattern

Photographs in Fig. 3 show the typical smoke-wire visualized characteristic flow patterns on the plane $Y/C = 3$, where the tip and wall effects are negligible. The chord Reynolds number is 3195. For flows in region A of Fig. 2, the laminar boundary layers on the suction and pressure sides of the airfoil are all attached to the surfaces. The typical smoke-wire flow pattern in this region is shown in Fig. 3a. No trace of separation is found. For flows in region B of Fig. 2, the laminar boundary layer on the suction surface separates,

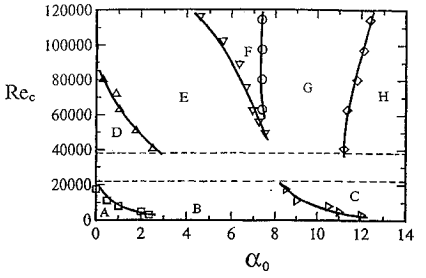

Fig. 2 Regions of characteristic flow modes on plane of $Y/C = 3$ in domain of chord Reynolds number and root angle of attack; low chord Reynolds number regions: region A boundary layer attached, region B boundary layer separated, region C boundary layer completely separated; and high chord Reynolds number regions: region D laminar separation, region E separation bubble, region F transition, region G turbulent separation, and region H three-dimensional flow.

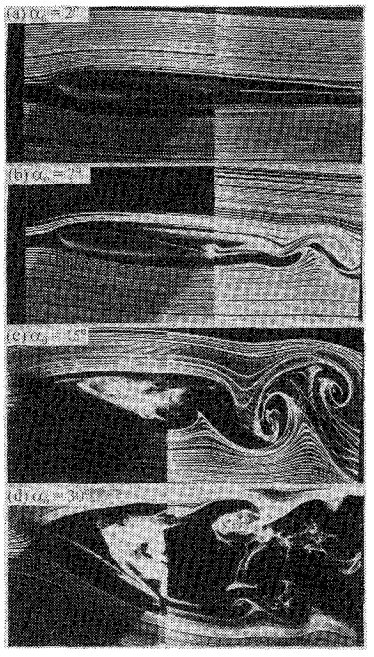

Fig. 3 Typical smoke-streak photographs for flows at low-Reynolds numbers: $Re_c = 3195$, smoke wires placed at $Y/C = 3$.

as shown in Fig. 3b. The separation starts from the trailing edge and moves toward the leading edge with increase of the root angle of attack. No reattachment of the separated boundary layer is found in this region. The unsteady flow structures are observed in the near wake region. The vortices shed alternatively from the upper shear layer of the separated boundary layer and the lower shear flow evolving from the trailing edge. At this low-root angle of attack, the vortices developed in the upper and lower shear layers do not coalesce into staggered von Kármán type[20] vortex pairs in the near wake region. In region C of Fig. 2, the boundary layer separates almost from the leading edge. The Reynolds number is much too low to form the separation bubble, since the turbulent momentum developed in the separated boundary layer is not strong enough to cause a reattachment.[12] The typical smoke streak pattern of the completely separated flow is shown in Fig. 3c. The reverse flow is marked by the smoke entrained from the smoke wire placed 0.5 mm downstream from the trailing edge. The mixing and fluctuation in the separated flow region are quite strong, compared to the flow in the outer region. The vortices in the near wake region have developed into a paired structure, which look like a von Kármán type vortex street. The ratio of the longitudinal to lateral spacing of the vortex pair in the near wake region is about 2.221, which is much higher than the theoretical value of 0.281 obtained by von Kármán[20] for the fully developed vortex street behind a circular cylinder. At further large root angle of attack, as shown in Fig. 3d, the upper and lower shear layers evolved from the leading and trailing edges, respectively, are

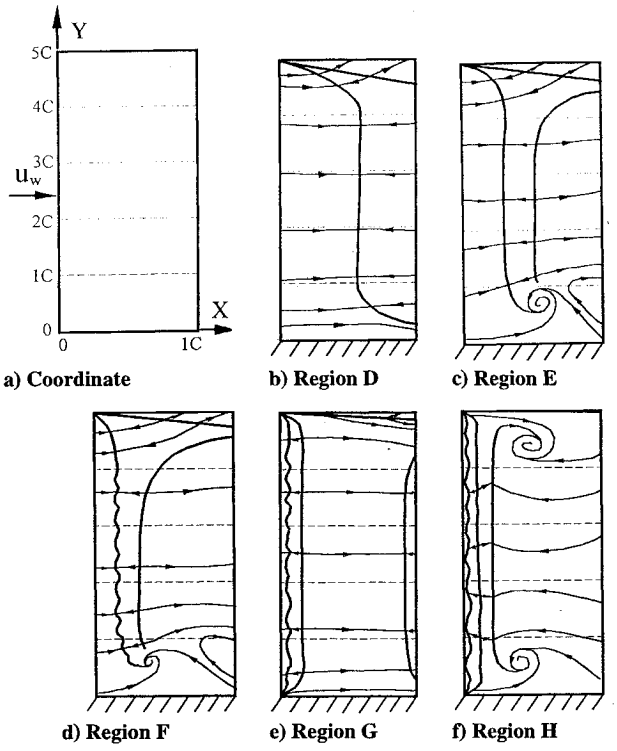

Fig. 4 Typical surface oil-flow patterns for flows in regions D–H of Fig. 2, Re_c = 80,185: a) coordinate, b) α_0 = 0.1 deg, c) α_0 = 5.0 deg, d) α_0 = 7.1 deg, e) α_0 = 8.8 deg, and f) α_0 = 12.5 deg.

widely spaced in the near wake region. The instability waves developed on the separated shear layers roll up to form vortices. At high-root angle of attack, which the bluff-body effect dominates, the large spacing between the shear flows evolved from the leading and trailing edges inhibits the direct interaction of the shear-layer instability waves. The low-frequency von Kármán type vortex shedding is superimposed by the high-frequency shear-layer instability waves.

Surface Oil-Flow Pattern

The surface oil-flow technique is applied to the regime where the chord Reynolds number is higher than 38,000. The sketches of Fig. 4 show the observed oil-flow patterns on the airfoil surface of suction side in each characteristic flow regime at chord Reynolds number 80,185. The coordinates and the approaching direction of the wind are shown in Fig. 4a. Figures 4b–4f correspond to the typical patterns in regions D–H in Fig. 2, respectively. The bold lines are where the massive dyed oil accumulated on the airfoil surfaces. The thin lines with arrow heads indicate the paths and directions of oil flow on the airfoil surface.

In Fig. 4b, which corresponds to region D of Fig. 2, the bold line stays approximately at where the boundary layer separates. The location of separation moves toward the leading edge with the increase of the root angle of attack or Reynolds number because the surface flow is still in the range of the laminar boundary layer. The surface oil flow in the attached flow area moves in the main stream direction. The surface oil flow moves toward the upstream direction after the separation of the boundary layer because of the reverse flow. The lateral spreading of turbulence from the side wall may delay the separation of the boundary layer. This wall effect causes the separation line to curve toward the trailing edge, as shown around the root area. No separation was found even in the area very close to the wall. Around the tip of the airfoil, the pressure gradient induced by the flow crossing the sharp corner may cause the local separation of the boundary layer. The end effect causes the separation line to curve toward the leading edge. Around the tip, the upright flow may be caused by the reattachment of the separated flow. Region D is called the laminar separation regime.

In Fig. 4c, which corresponds to region E of Fig. 2, the left bold line is where the boundary layer separates, whereas the right one represents where the separated flow reattaches. A separation bubble must exist between these two bold lines. The bubble moves toward the leading edge and becomes smaller with the increase of root angle of attack. Near the root area, the separated boundary layer does not reattach due to the wall effect. The reverse flow from the trailing edge together with the forward flow from the leading edge generates a surface vortex near the root area. Around the tip area, the end effect causes the advance of separation and the delay of reattachment. Hence, the separation line curves toward the leading edge and the reattaching line toward the trailing edge. The upper right flowing area around the tip shrinks with the increase of the root angle of attack. Region E is called the separation bubble regime.

In Fig. 4d, which corresponds to region F of Fig. 2, the separation line becomes wavy. Both the separation and reattaching lines move toward the leading edge with the increase of root angle of attack. The effects of the wall and the tip on the flow are similar to those in region E, except that the location of the surface vortex moves toward the root of the airfoil because the separation line extends toward the root with the increase of root angle of attack. The upper right flowing area around the tip shrinks further as the root angle of attack is increased. Region F is a transitional regime.

In Fig. 4e, which corresponds to region G of Fig. 2, the wavy separation line stays very close to the leading edge and does not appreciably move with the increase of root angle of attack. A short leading-edge separation bubble is formed. The surface vortex disappears since the separation and reattaching lines extend very close to the wall. The reattached boundary layer separates again and forms a second separation line. This second separation line moves toward the leading edge with the increase of root angle of attack. Region G is called the turbulent separation regime.

In Fig. 4f, which corresponds to region H of Fig. 2, a strong three-dimensional flow pattern is observed. Two surface vortices, one near the root area and the other near the wing tip, are generated due to the strong wall and end effects. Region H is called the three-dimensional flow regime.

The observed three-dimensional separated flow pattern, in which a system of vortices develops with vortex filaments not everywhere aligned to the oncoming flow, is quite similar to that reported by Bippes.[21] At this high angle of attack and Reynolds number, the trace of the downwash effect by the spiral tip vortex is not appreciably found on the tip area of the suction side surface. Obviously, the depth of influence caused by the tip vortex decreases with the increase of root angle of attack on the wing surface. It may be caused by the fact that the wing is stalled and, therefore, the tip vortices are weak.

Wake Structure

The smoke-wire visualized flow structures in the wake region of the airfoil on the $Y/C = 3$ plane are shown in Fig. 5. The chord Reynolds number is 3195. At $\alpha_0 = 0$ deg, where no photograph is shown, the flow in the wake region remains smooth. The

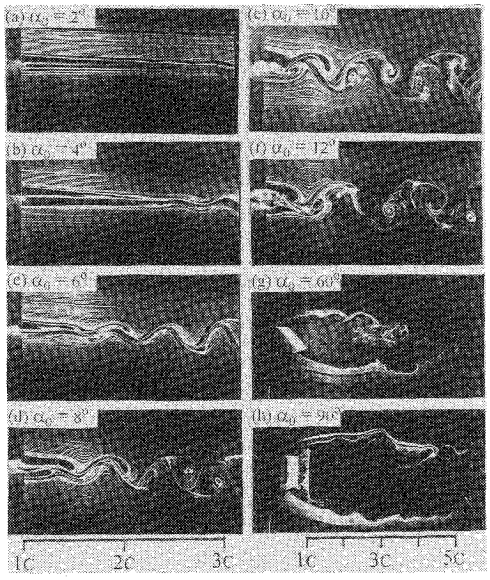

Fig. 5 Typical smoke-wire visualized unsteady flow structures in wake region: Re_c = 3195, smoke wires placed at Y/C = 3.

Kutta–Joukowsky condition[22] should apply properly. At $\alpha_0 = 2$ deg, as shown in Fig. 5a, the unstable waves in the shear layer are observed for $X/C > 2$. Although not shown in Fig. 5a, the unstable waves are amplified as they propagate farther downstream. At $\alpha_0 = 4$ deg, the suction side boundary layer starts to separate from the trailing edge. The upper and lower shear-layer instability waves, developed in the suction side separated boundary layer as well as in the pressure side separated shear flow from the trailing edge, have a small phase difference in the near wake region. The phase difference and the amplitude enlarge as the waves propagate downstream. The unstable waves eventually develop into alternatively shed von Kármán type vortices in the far downstream region for $X/C > 4$, which is not shown in the figure. In Figs. 5c and 5d for $\alpha_0 = 6$ and 8 deg, respectively, vortices with small phase differences are formed in the near wake region. The location of inception of the von Kármán type vortex shedding moves upstream with increase of the root angle of attack. For higher root angles of attack, as shown in Figs. 5e and 5f for $\alpha_0 = 10$ and 12 deg, the von Kármán type vortex shedding starts earlier from about $X/C = 1.4$. In our observation, for root angle of attack lower than about 25 deg, the vortex shedding is developed from the interaction of the upper and lower shear layers, as already stated. For root angle of attack higher than about 25 deg, as shown in Figs. 5g and 5h for $\alpha_0 = 60$ and 90 deg, the large spacing between the shear layers evolved from the leading and trailing edges inhibits the direct interaction of the instability waves. The von Kármán type vortex shedding, although not observable via the smoke streaks in Figs. 5g and 5h, can be detected by the hot-wire anemometer placed at far downstream locations. The shedding frequency of the von Kármán type vortex street at high root angle of attack is much lower than that at low root angle of attack, and the frequency of the traveling vortices developed from the shear layer instability waves is much higher than that of the von Kármán type vortex street. The bluff-body effect induced separation and the large pressure gradient should be responsible for the low-frequency vortex shedding formed in the downstream area.

Vortex Shedding Characteristics

Characteristic Modes of Vortex Shedding

The shed vortices in the wake region behind the airfoil present the behaviors similar to the four characteristic modes, laminar, subcritical, transitional, and supercritical of the von Kármán vortex street behind the circular cylinder which was observed by Lienhard.[23] Regions I, II, III, and IV of Fig. 6 correspond to the laminar, subcritical, transitional, and supercritical flow modes, respectively, in the wake region behind the airfoil at $Y/C = 3$. The typical hot-wire signals for these four modes detected at $Y/C = 3$ and $X/C = 2$ are shown in Fig. 7. At low-wind velocity and root angle of attack, as in the region I of Fig. 6, the hot-wire output signal is smooth and periodic, as shown in Fig. 7a. The shed vortices are in the laminar mode. The regime for the laminar shedding mode in Fig. 6 corresponds to the characteristic flow regions where the laminar boundary layer is either attached to or separated from the suction surface of the airfoil in Fig. 2. In this regime, the instabilities do not develop in the upper and lower shear layers. In region II of Fig. 6, the hot-wire output signals become fluctuating, as shown in Fig. 7b. The periodic signal of the shed vortices is superimposed by the fluctuations. The vortices are in the subcritical shedding mode. Compared to Fig. 2, the vortex shedding in the subcritical mode is observed either when the separated boundary layer reattaches to the suction surface of the airfoil to form the recirculation bubble at high chord Reynolds numbers or when the flow in the separated boundary layer becomes unstable at low-chord Reynolds numbers. In this regime, the turbulent fluctuations are found in the vortices due to the instabilities developed in the upstream flow structures. With the increase of the chord Reynolds number or root angle of attack, the intensity of the turbulence amplifies and the periodicity of the vortex shedding decreases. In region III of Fig. 6, the hot-wire output signals become irregular, as shown in Fig. 7c. The shed vortices lose coherency, and the flow structure in the wake is disorganized. No peak value is found in the power spectrum of the hot-wire signal. The shed vortices are in the transitional mode. In this regime, the coherency of the organized structures in the wake region is not sustained, probably due to

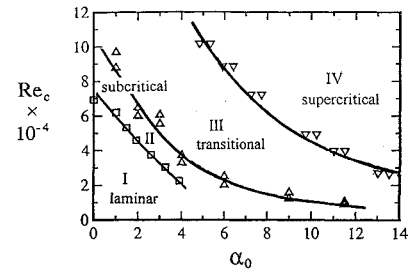

Fig. 6 Classification of characteristic vortex shedding modes in the domain of chord Reynolds number and root angle of attack.

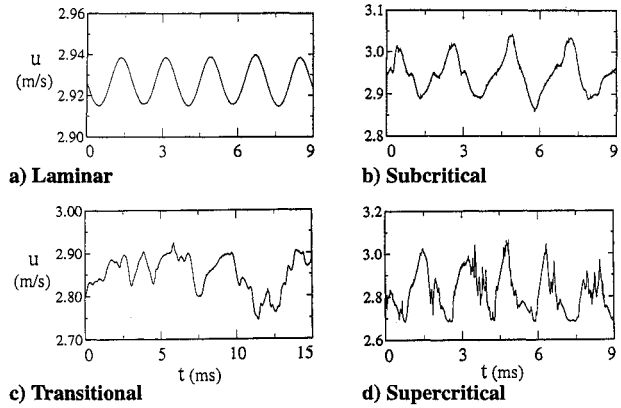

Fig. 7 Typical hot-wire signals for vortex shedding in four characteristic modes, Re_c = 27,610: a) α_0 = 1 deg, b) α_0 = 4.5 deg, c) α_0 = 8 deg, and d) α_0 = 16 deg.

the effects of mixing and the momentum exchange induced by the strong turbulent fluctuations developed in the boundary layer downstream the reattachment point. The enhanced turbulence intensity may smear and break up the large structures in the flow. In region IV of Fig. 6, the hot-wire signal becomes periodic again, although superimposed by large turbulent fluctuations, as shown in Fig. 7d. The turbulent vortex shedding is re-established. A peak value is found in the power spectrum of the hot-wire signal. The shed vortices are in the supercritical mode. In this regime, turbulent vortex shedding is reestablished through a turbulent boundary-layer separation, as has been reported by Roshko.[24] Apparently, the characteristic modes of the vortex shedding in the wake region are closely related to the behaviors of the boundary layer on the suction surface of the airfoil.

Frequency of Vortex Shedding

Figure 8 shows the variation of the frequency of the vortex shedding in the wake region behind the airfoil with freestream velocity for various root angles of attack. The hot wire is placed on the $Y/C = 3$ plane and two chord lengths in the downstream area of the leading edge. For root angle of attack lower than 9 deg, as shown in the upper four curves in Fig. 8a, the vortex shedding is detected basically in the laminar and subcritical regimes of Fig. 6. The frequency of the vortex shedding increases sharply with the increase of freestream velocity. The increase rate increases with wind velocity and decreases with root angle of attack. For root angle of attack higher than 15 deg, as shown in Fig. 8b, the vortex shedding detected is basically in the supercritical regime of Fig. 6. The frequency of the vortex shedding increases linearly with the increase of freestream velocity. The decrease rate of the vortex shedding frequency decreases with the increase of root angle of attack. The variation of the Strouhal number of the vortex shedding frequency with the chord Reynolds number is shown in Fig. 9. In the laminar regime, the Strouhal number increases with the increase of chord Reynolds number. At $\alpha_0 = 0$ deg, the Strouhal number may even reach about 0.6, as shown in Fig. 9a. While in the supercritical regime, the Strouhal number approaches to a constant for a fixed root angle of attack, as shown in Fig. 9b. The constants of the Strouhal number in the supercritical regime range from 0.12 to 0.22. The

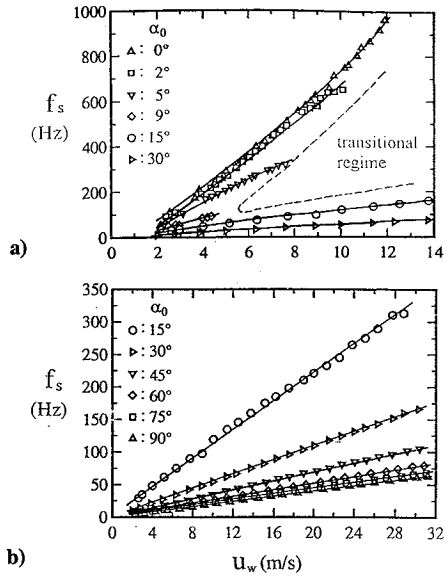

Fig. 8 Variation of vortex shedding frequency with freestream velocity, data measured at Y/C = 3 and X/C = 2: a) low angles of attack and b) high angles of attack.

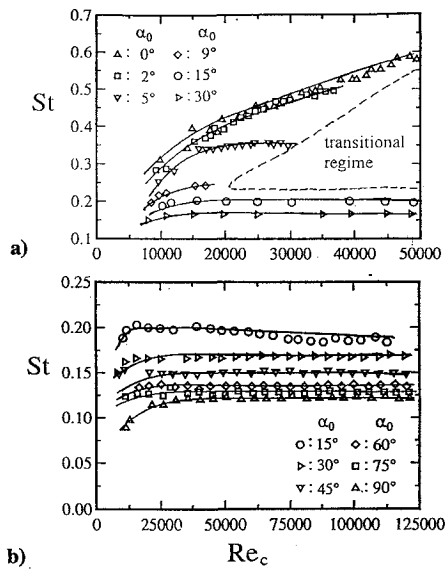

Fig. 9 Variation of Strouhal number of vortex shedding with chord Reynolds number, data measured at Y/C = 3 and X/C = 2: a) low angles of attack and b) high angles of attack.

higher the root angle of attack is, the lower the value of the constant is. The variation of the Strouhal number with the root angle of attack is shown in Fig. 10. The Strouhal number, at any chord Reynolds number, decreases with the increase of root angle of attack. For root angle of attack higher than about 15 deg, the Strouhal numbers at different Reynolds numbers gradually collapse to a narrowband and the decrease rate with the root angle of attack slows. For root angle of attack higher than about 25 deg, the variation of the Strouhal number with the root angle of attack becomes limited. This may be induced primarily by the enhancement of the bluff-body effect, that is, the upper and lower shear layers are spaced too far apart to interact directly with each other as stated in the section on wake structure.

The effects of the tip and wall on the shedding frequency are shown in Fig. 11. At low root angle of attack in the regime of the laminar shedding mode, the shedding frequency varies with the span location, as shown in Figs. 11a and 11b. The vortex shedding has lower frequency around the root and tip areas compared to the central region. The advance of the separation around the wing tip due to the existence of tip vortex as well as the deceleration of the flow around the root area may cause the decrease of the vortex

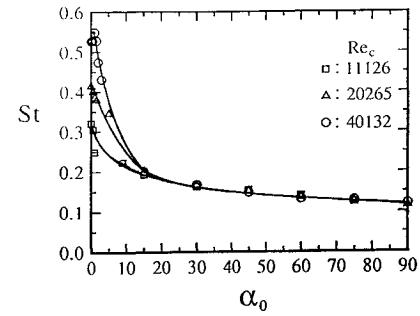

Fig. 10 Variation of Strouhal number of vortex shedding with root angle of attack, data measured at X/C = 2.

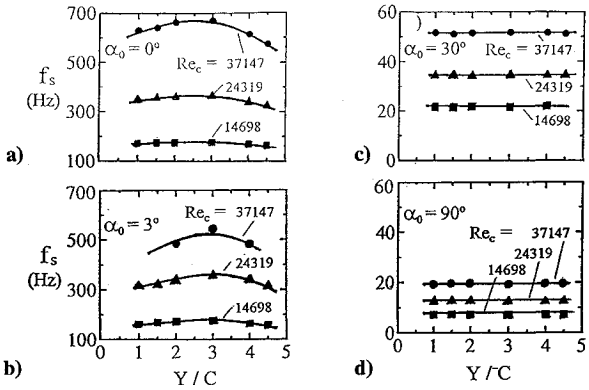

Fig. 11 Influences of juncture and wing tip on the frequency of vortex shedding, data measured at Y/C = 3 and X/C = 2: a) α_0 = 0 deg, b) α_0 = 3 deg, c) α_0 = 30 deg, and d) α_0 = 90 deg.

shedding frequency. The higher the chord Reynolds number or root angle of attack is, the more obvious the decrease is. The maximum value exists from Y/C = 2–3. The position of the maximum moves toward the tip direction with the increase of root angle of attack; at high root angle of attack in the regime of supercritical shedding mode, as shown in Figs. 11c and 11d, no appreciable influence of the tip and wall on the shedding frequency is detected for Y/C between 1 and 4.5. The bluff-body effect at high angle of attack reduces the influence of the tip vortex on the surface boundary layer. The turbulence transition around the root area has less influence on the boundary layer. These may lead to the uniform distribution of the shedding frequency along a large part of the wing span.

Characteristics of Shear-Layer Instabilities

In the smoke-streak visualized flow pattern, as shown in Figs. 3 and 5, the vortex shedding at low-root angles of attack in the wake region has been found to be evolving from the shear-layer instabilities. At high-root angles of attack, where the bluff-body effect dominates, the low-frequency vortex shedding is superimposed by the high-frequency shear layer instability waves. The frequencies of the upper shear-layer instability waves at low angles of attack on the Y/C = 3 plane are detected by placing a hot-wire probe at X/C = 1. The detected frequencies of the shear-layer instability waves for freestream velocity lower than 28 m/s at low-root angles of attack are presented in Fig. 12. The regions separated by the dashed lines correspond to the laminar, subcritical, and transitional characteristic modes in Fig. 6. In the laminar region, the stable frequencies of the shear-layer instabilities are obtained. The solid lines indicate this feature. The frequencies of the shear-layer instabilities presented in Fig. 12 are much higher than those of the vortex shedding in the wake shown in Fig. 8a. The frequency decreases with the increase of root angle of attack. In the transitional region, the frequency of the shear-layer instabilities becomes unstable. The frequency distributes across the shaded areas. This may cause the vortices in the wake to transition from the laminar to the subcritical mode. In the subcritical region, no steady single-valued peak in the spectrum is found. The irregularity in the shear layer causes the loss of coherency of the vortices in the wake region. Apparently, at low angles of attack, the characteristic

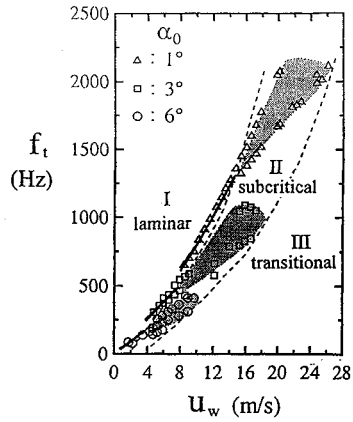

Fig. 12 Variation of frequency of shear-layer instability waves with freestream velocity at low angles of attack.

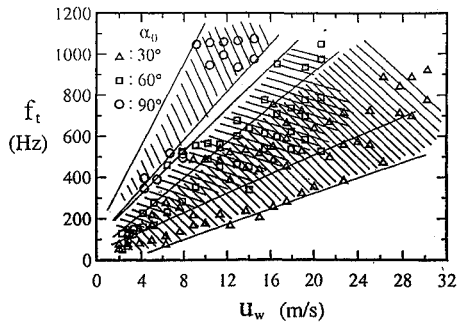

Fig. 13 Variation of frequency of shear-layer instability waves with freestream velocity at high angles of attack.

vortex modes are closely related to the behavior of the shear-layer instabilities. At the high angles of attack, where the bluff-body effect becomes important, the hot-wire probe placed at $X/C = 2/3$ detects multifrequency again, as shown in Fig. 13. The higher the freestream velocity, the wider the frequency distribution appears. The frequencies increase with the increase of root angle of attack. The irregular high-frequency shear-layer instabilities seem to have less interconnection with the low-frequency vortex shedding in the wake region, as compared with Fig. 8.

Concluding Remarks

The characteristics of the flow patterns and unsteady flow structures of a NACA 0012 cantilever airfoil have been studied experimentally. The smoke streaks and surface oil-flow observations delineate the existence of several characteristic flow modes in the chord Reynolds number/root angle-of-attack domain. The characteristic flow modes include laminar separation, separation bubble, transitional, turbulent separation, and three-dimensional modes. The surface vortices, which characterize the three-dimensional flow patterns on the airfoil surface, are found to be profoundly influenced by the wall and tip effects. The evolution of the vortex shedding behind the airfoil at low angle of attack is found to be closely related to the behavior of the shear-layer instabilities. At high angle of attack, the low-frequency shedding is superimposed by the high-frequency shear layer instability waves. Four characteristic modes of vortex shedding are found in the chord Reynolds number/root angle-of-attack domain. They are the laminar, subcritical, transitional, and supercritical modes. These characteristic shedding modes are closely related to the behaviors of the boundary layer on the suction surface. The shedding frequency increases with the increase of chord Reynolds number and decreases with the increase of root angle of attack. The wall and wing tip reduce the frequency of vortex shedding via different mechanisms. The behaviors of the shear-layer instabilities correspond to the characteristic regimes of the vortex shedding. At low angle of attack, the shear-layer instability waves are basically stable only in the laminar shedding regime. The shear-layer instability frequency decreases with the increase of root angle of attack. At high angle of attack, where the bluff-body effect dominates, no unique wave frequency is found.

Acknowledgments

This study was supported by the National Science Council of the Republic of China under Grant NSC 84-2212-E-011-040. The authors appreciate the help of David Han for suggestions of instrumentation and the help of M. Z. Lin for the construction of the wind tunnel.

References

[1]Crabtree, L. F., "Effects of Leading-Edge Separation on Thin Wings in Two-Dimensional Incompressible Flow," *Journal of the Aeronautical Sciences*, Vol. 24, No. 8, 1957, pp. 597–604.

[2]Ward, J. R., "The Behavior and Effects of Laminar Separation Bubbles on Airfoils in Incompressible Flow," *Journal of the Royal Aeronautical Society*, Vol. 67, Dec. 1963, pp. 783–790.

[3]Arena, A. V., and Mueller, T. J., "Laminar Separation, Transition, and Turbulent Reattachment near the Leading Edge of Airfoils," *AIAA Journal*, Vol. 18, No. 7, 1980, pp. 747–753.

[4]Batill, S. M., and Mueller, T. J., "Visualization of Transition in the Flow over an Airfoil Using the Smoke-Wire Technique," *AIAA Journal*, Vol. 19, No. 3, 1981, pp. 340–345.

[5]Mueller, T. J., and Batill, S. M., "Experimental Studies of Separation on a Two-Dimensional Airfoil at Low Reynolds Numbers," *AIAA Journal*, Vol. 20, No. 4, 1982, pp. 457–463.

[6]Mueller, T. J., Pohlen, L. J., Conigliaro, P. E., and Jansen, B. J., Jr., "The Influence of Free-Stream Disturbances on Low Reynolds Number Airfoil Experiments," *Experiments in Fluids*, Vol. 1, No. 1, 1983, pp. 3–14.

[7]Pohlen, L. J., and Mueller, T. J., "Boundary Layer Characteristics of the Miley Airfoil at Low Reynolds Numbers," *Journal of Aircraft*, Vol. 21, No. 9, 1983, pp. 658–664.

[8]Mueller, T. J., "The Influence of Laminar Separation and Transition on Low Reynolds Number Airfoil Hysteresis," *Journal of Aircraft*, Vol. 22, No. 9, 1985, pp. 763–770.

[9]Marchman, J. F., "Aerodynamic Testing at Low Reynolds Numbers," *Journal of Aircraft*, Vol. 24, No. 2, 1987, pp. 107–114.

[10]O'Meara, M. M., and Mueller, T. J., "Laminar Separation Bubble Characteristics on an Airfoil at Low Reynolds Numbers," *AIAA Journal*, Vol. 25, No. 8, 1987, pp. 1033–1041.

[11]Hsiao, F.-B., Liu, C.-F., and Tang, Z., "Aerodynamic Performance and Flow Structure Studies of a Low Reynolds Number Airfoil," *AIAA Journal*, Vol. 27, No. 2, 1989, pp. 129–137.

[12]Lissaman, P. B. S., "Low Reynolds Number Airfoils," *Annual Review of Fluid Mechanics*, Vol. 15, 1983, pp. 223–239.

[13]Zaman, K. B. M., McKinzie, D. J., and Rumsey, C. L., "A Natural Low-Frequency Oscillation of the Flow over an Airfoil near Stalling Conditions," *Journal of Fluid Mechanics*, Vol. 202, May 1989, pp. 403–442.

[14]Stuber, K., and Gharib, M., "Experiment on the Forced Wake of an Airfoil Transition from Order to Chaos," AIAA Paper 88-3840, 1988.

[15]Blevins, R. D., *Flow-Induced Vibration*, 2nd ed., Van Nostrand Reinhold, New York, 1990, pp. 43–104.

[16]Bollay, W., and Brown, C. D., "Some Experimental Results on Wing Flutter," *Journal of the Aeronautical Sciences*, Vol. 8, No. 5, 1941, pp. 313–318.

[17]Bejan, A., *Convection Heat Transfer*, Wiley, New York, 1984, pp. 110–114.

[18]Mueller, T. J., "Flow Visualization by Direct Injection," *Fluid Mechanics Measurements*, 1st ed., edited by R. J. Goldstein, Hemisphere, New York, 1983, pp. 307–340.

[19]Flagan, R. C., and Seinfeld, J. H., *Fundamentals of Air Pollution Engineering*, Prentice–Hall, Englewood Cliffs, NJ, 1988, pp. 295–307.

[20]Von Kármán, T., *Collected Works of Theodore von Kármán*, Vol. 1, Butterworths, London, 1956, pp. 331–338.

[21]Bippes, H., "Experimental Investigation of Topological Structure in Three-dimensional Separated Flow," *Proceeding of the 26th Internation Union of Theoretical and Applied Mechanics Symposium*, Springer–Verlag, Berlin, 1987, pp. 379–381.

[22]Abbott, I. H., and von Doenhoff, A. E., *Theory of Wing Section*, Dover, New York, 1959, pp. 50–53.

[23]Lienhard, J. H., "Synopsis of Lift, Drag, and Vortex Frequency Data for Rigid Circular Cylinders," Washington State Univ., Research Div. Bulletin 300, College of Engineering, Seattle, WA, 1966.

[24]Roshko, A., "Experiments on the Flow Past a Circular Cylinder at Very High Reynolds Number," *Journal of Fluid Mechanics*, Vol. 10, May 1961, pp. 345–356.